Neonatal brain segmentation using second order neighborhood information

Christian Ledig*, Robert Wright*, Ahmed Serag*, Paul Aljabar†,*, Daniel Rueckert*

* Department of Computing, Imperial College London, London, UK
† Imaging Sciences and Biomedical Engineering, Kings College London, London, UK

Abstract. The dynamic contrast changes in T_2-weighted magnetic resonance (MR) images in developing brains are one of the main reasons that make tissue segmentation in neonatal MR brain scans very challenging. However, to assess and understand early brain development, it is crucial to be table to robustly and accurately segment neonatal MR images. It is especially the varying intensity profile from white matter (WM) to grey matter (GM) to cerebrospinal fluid (CSF) that hampers the direct application of intensity based segmentation algorithms such as the expectation-maximization (EM) algorithm. In this work, we present an approach that incorporates prior spatial information by using a 4D probabilistic spatio-temporal atlas and extends the widely used EM algorithm by an energy function that penalizes implausible neighborhood configurations. Inspired by the Markov Random Field (MRF) that is described by a connectivity matrix, we introduce a connectivity tensor that allows the incorporation of second order neighborhood information. We evaluate our approach by careful visual inspection and by a measure based on the number and size of connected WM components.

1 Introduction

During the rapid and complex brain growth before and after birth, morphological, appearance and functional brain properties change dramatically [1]. The detection of abnormal brain development during the early phase of life in infants born prematurely is both an important and challenging problem [2–4]. Due to better contrast and structural information, tissue segmentation algorithms designed for neonatal images are usually based on T_2-weighted MR images (MRI) [5]. As shown in [3], the intensity distribution of different brain tissue classes changes severely shortly after birth. It is because of this substantial intensity variation in early development that purely intensity-based methods such as [5] are prone to systematic misclassifications resulting from overlaps in tissue distributions of the white matter (WM) and grey matter (GM) class. However, many approaches for the assessment of brain development are based on the distribution of different types of brain tissue, such as WM, GM or also cerebrospinal fluid (CSF) [3, 4, 6, 7]. Atlases that provide prior spatial inforation are used to address the problems of a sole intensity-based segmentation algorithm [2–5].

In this work we focus on the problem of wrongly labeled partial volume (PV) voxels on the cortical GM (cGM) boundary. Due to PV effects and the T_2-specific intensity distribution both CSF and cGM voxels on the outer cGM boundary tend to be wrongly classified as WM (Fig. 1). This issue has been addressed in [5] where wrongly classified voxels are detected and relabeled by relaxing the MRF weights. Similarly [4] approached this problem by modifying spatial priors in iterative relaxation steps.

Our approach aims in the same direction, however instead of relying solely on a relaxation in each iteration we incorporate second order neighborhood information through a 3-tensor directly into the EM energy formulation. This sets our method apart from previously published EM variants [4, 8, 9]. With this formulation we avoid unreasonably high MRF weights, which allow the suppression of misclassification of small voxel patches but at the expense of segmentation accuracy at other boundaries. This makes our model very general. It is also adaptable to other segmentation challenges, such as structural adult brain segmentation.

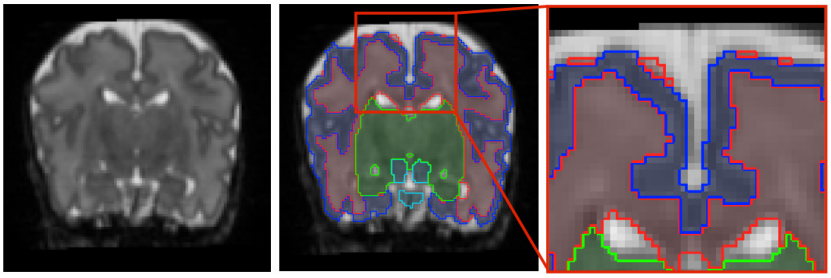

Fig. 1. T_2-weighted MR scan (34 weeks GA, left) with overlaid automatic segmentation (middle). Region of interest with wrongly labeled PV voxels (right). WM: red, cGM: dark blue, dGM: green, BS: light blue.

2 Method

2.1 Data and Preprocessing

A first step in preparing the neonatal T_2-weighted MRI scans for segmentation is the masking of non-brain tissues in all images in the database. The Brain Extraction Tool (BET) is used [10] to remove all non-brain tissue in each image. In a subsequent step, images were corrected for intensity inhomogeneity using the N4 algorithm [11]. We then co-aligned all images, dependend on the subjects age, to their corresponding time frame of a spatio-temporal atlas [4] for which age-dependent average templates and tissue probability maps, in an age range of 29-44 weeks of gestation, are available. Subjects used in evaluation were not used in the atlas construction process. The atlas provides probability maps for seven

classes which are namely: white matter (WM), cortical grey matter (cGM), deep grey matter (DGM), cerebrospinal fluid (CSF), cerebellum (CB), brainstem (BS) and background (BG).

For evaluation we segmented 71 T_2-weighted MR scans of neonates with a gestational age (GA) between 27-48 weeks (38±5.7). For subjects younger than 29 or older than 44 weeks GA we used the atlas frames of 29 weeks GA and 44 weeks GA respectively. All MRI scans were acquired on a 3 Tesla Philips Intera system with parameters: T_2-weighted fast spin-echo, TR=8700 ms, TE=160 ms, flip angle=90°, axial acquisition plane, voxel size=1.15x1.18x2 mm, FOV=220 mm and an acquired matrix of 192x186 voxels.

2.2 Intensity Model and ML Approach

We index the n voxels of a T_2-weighted MRI scan $\mathbf{I}$ by $i = 1, \ldots, n$, so that for intensities $y_i \in \mathbb{R}$ the image is defined as $\mathbf{I} = \{y_1, y_2, \ldots, y_n\}$. We denote the corresponding probabilistic segmentation as $\mathbf{Z} = \{\mathbf{z}_1, \mathbf{z}_2, \ldots, \mathbf{z}_n\}$, where $\mathbf{z}_i$ is a vector of size K and the k^{th} component represents the probability that a voxel belongs to tissue class k. We also follow the approach of van Leemput et al. [8] and estimate the underlying but unknown segmentation $\mathbf{S}_{\text{prob}}$ by means of the observed intensities $\mathbf{y}$. Assuming that the observed log-transformed intensities of voxels belonging to class k are normally distributed with mean μ_k and standard deviation σ_k, the overall model parameters are given as $\mathbf{\Phi} = \{(\mu_1, \sigma_1), (\mu_2, \sigma_2), \ldots, (\mu_K, \sigma_K)\}$. In case of known parameters $\mathbf{\Phi}$ the probability of observing an intensity y_i at voxel i can be computed as:

$$f(y_i|\mathbf{\Phi}) = \sum_k f(y_i|\mathbf{z_i} = \mathbf{e_k}, \mathbf{\Phi}) f(\mathbf{z_i} = \mathbf{e_k}) \tag{1}$$

Here $f(\mathbf{z_i} = \mathbf{e_k})$ is the probability of voxel i having tissue class k and $f(y_i|\mathbf{z_i} = \mathbf{e_k}, \mathbf{\Phi})$ is a Gaussian distribution with parameters (μ_k, σ_k). At this point we assume statistical independence between all voxels. The overall probability of observing an image $\mathbf{y}$ with known parameters $\mathbf{\Phi}$ can then be written as $f(\mathbf{y}|\mathbf{\Phi}) = \prod_i f(y_i|\mathbf{\Phi})$. We apply the EM algorithm by interleaving the expectation of the class probabilities $p_{ik}^{(m+1)}$, while assuming that the model parameters $\mathbf{\Phi}$ are fixed, and the maximization of $f(\mathbf{y}|\mathbf{\Phi})$ by varying the model parameters. m denotes the iteration number. In order to account for topological and spatial apriori knowledge this model can be further modified by employing MRFs. This is done by expanding $f(\mathbf{z_i} = \mathbf{e_k})$ to

$$f(\mathbf{z_i} = \mathbf{e_k}|p_{\mathcal{N}_i}^{(m)}) = \frac{\pi_{ik} e^{-U_{\text{MRF}}(\mathbf{e_k}|p_{\mathcal{N}_i}^{(m)})}}{\sum_{j=1}^{K} \pi_{ik} e^{-U_{\text{MRF}}(\mathbf{e_k}|p_{\mathcal{N}_i}^{(m)})}} \tag{2}$$

where π_{ik} is an anatomical probabilistic prior for class k at voxel i and $\mathcal{N}_i$ is the set of first-order neighbours of voxel i. We follow the approach of a global and

stationary MRFs as proposed in [9] and employ the energy function

$$U_{\mathrm{MRF}}(\mathbf{e_k}|p_{\mathcal{N}_i}^{(m)}) = \sum_{j=1}^{K} G_{kj} v_j \tag{3}$$

where $\mathbf{G}$ denotes a $K \times K$ matrix defining the connectivity between class k and j. The column vector $\mathbf{v}$ of size K denotes the accumulated class probabilities in the 6-neighborhood $\mathcal{N}_i$ of voxel i. Thus the k-th component of $\mathbf{v}$ is calculated as

$$v_k = (\sum_{l \in \mathcal{N}_i^x} s_x p_{lk} + \sum_{l \in \mathcal{N}_i^y} s_y p_{lk} + \sum_{l \in \mathcal{N}_i^z} s_z p_{lk}) \tag{4}$$

where $s = \{\frac{1}{d_x}, \frac{1}{d_y}, \frac{1}{d_z}\}$ accounts for the anisotropic voxel spacing in the images. We extend this model further by incorporating second order neigborhood information into the standard model by extending $f(\mathbf{z_i} = \mathbf{e_k})$ to

$$f(\mathbf{z_i} = \mathbf{e_k}|p_{\mathcal{N}_i}^{(m)}) = \frac{\pi_{ik} e^{-U_{\mathrm{MRF}}(\mathbf{e_k}|p_{\mathcal{N}_i}^{(m)})} e^{-U_{2\mathrm{nd}}(\mathbf{e_k}|p_{\mathcal{N}_i}^{(m)})}}{\sum_{j=1}^{K} \pi_{ik} e^{-U_{\mathrm{MRF}}(\mathbf{e_k}|p_{\mathcal{N}_i}^{(m)})} e^{-U_{2\mathrm{nd}}(\mathbf{e_k}|p_{\mathcal{N}_i}^{(m)})}} \tag{5}$$

where we introduce a novel energy function $U_{2\mathrm{nd}}$ defined as:

$$U_{2\mathrm{nd}}(\mathbf{e_k}|p_{\mathcal{N}_i}^{(m)}) = \mathbf{v}^{\mathrm{T}} \mathbf{T}_k \mathbf{v} \tag{6}$$

Here, $\mathbf{T}_k$ is a matrix representing the k-th slice of the 3-tensor T_{kjl} that penalizes implausible neighborhood configurations of a class k. In particular, if class k is expected to be adjacent both to class j and l, the component $\mathbf{T}_{\mathrm{kjl}}$ equals zero (no penalty). While the standard MRF energy function as shown in Equation 3 penalises any presence of class j in the neighborhood of a label k, the second order energy function introduced in Equation 6 penalises the presence of class j in the neighborhood of label k if and only if class l is present as well.

In addition we explicitly model PV voxels based on the approach presented in [9]. We derive the MRF properties of the PV classes from $\mathbf{G}$ and $\mathbf{T}$. By extending the connectivity matrix $\mathbf{G}$ we model a PV class distant to all classes except the two adjacent parent classes between which the PV class is modeled. The second order neighborhood constraints for the PV class are directly inherited from both parent classes. We thus set the matrix $\mathbf{T}_{\mathrm{pvAB}} = \mathbf{T}_{\mathrm{parentA}} + \mathbf{T}_{\mathrm{parentB}}$. Since the used atlas provides priors for $K = 7$ classes, we model these seven different tissue types with a single Gaussian distribution each.

3 Experimental Results

3.1 Evaluation Strategy and Parameters

We evaluated the presented EM-based segmentation algorithm with and without the incorporation of second order neighborhood information using the introduced

tensor $\mathbf{T}$. Furthermore, we evaluate both version with and without explicit PV modeling. In total we compare four different setups of the EM algorithm: MRF without (MRF) and with explicit PV modeling (MRF PV), MRF with second order neighborhood information without (Proposed) and with explicit PV modeling (Proposed PV). When PV modeling is used we modeled three PV classes between (cGM,CSF), (WM,cGM) and (CSF,BG). To identify adjacent tissue classes for the MRF, we count the frequency of the labels of adjacent voxels in an existing automatic segmentation. After thresholding we obtained a 7×7 adjacency matrix $\mathbf{G}$ (see Eq. 3) that describes the MRF, with entry (i, i) equals 0 and entry (i, j) defined as 0.5 if structures i and j share a boundary and 1.5 if structures i and j are distant.

For neonatal tissue segmentation we add two constraints to the model using $\mathbf{T}$. We penalize the labeling of a WM voxel if the neighborhood indicates a high probability for both cGM and CSF voxels. We also penalize the labeling of a voxel as CSF in the neighborhood of both cGM and WM. We thus heuristically set $\mathbf{T}_{\text{WM,cGM,CSF}} = \mathbf{T}_{\text{WM,CSF,cGM}} = 1.5$ and $\mathbf{T}_{\text{CSF,cGM,WM}} = \mathbf{T}_{\text{CSF,WM,cGM}} = 1.5$.

Since no manual ground truth segmentations were available, we evaluated the suggested approach two-fold. First of all we conducted a visual inspection were we focused on the cortical region looking for wrongly labeled WM on the outer boundary of the cortex and CSF. In a second experiment we then calculated number and size of connected WM components, where we focused on components with unexpected neighborhood configurations.

3.2 Visual Inspection

For visual inspection we focused on the surface of segmentations obtained with different segmentation techniques. To investigate the outer cGM boundary we did not render CSF and the background label. The visual results for a random subject with a GA of 34 weeks is shown in Fig. 2. Comparing approaches with-

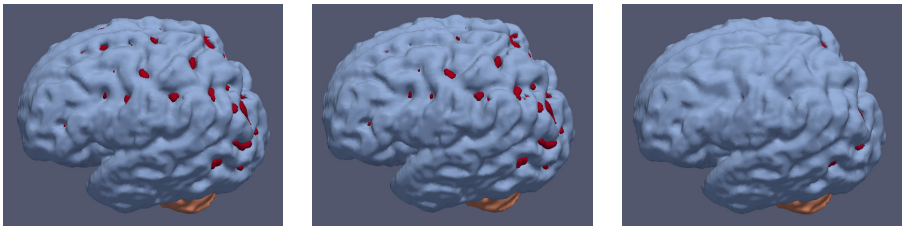

Fig. 2. Rendered segmentation results (subject: 34 weeks GA) for WM: red, cGM: blue, CB: orange. Methods: MRF (left), MRF (PV) (middle), Proposed (right).

out (left, middle) and with (right) the additional second order neighborhood constraints, we observe a considerable reduction in number of undesired WM

components on the outer surface of the cortical grey matter. The segmentations shown in Fig. 3 illustrate exemplary PV effects and how they are resolved using second order neighborhood information. We observed no significant visual difference whether explicit PV modeling is used (middle) or not (left).

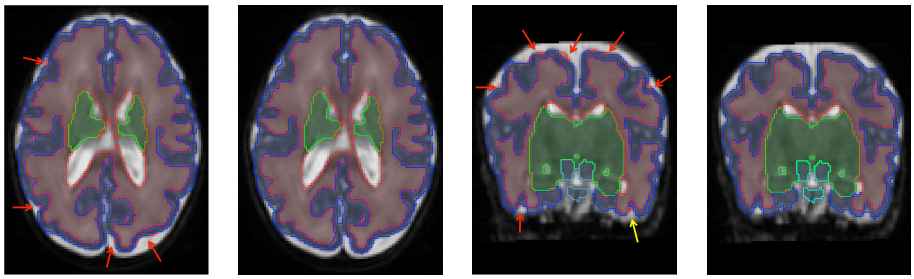

Fig. 3. Axial (left pair) and coronal (right pair) view of T_2-weighted MRI scan (34 weeks GA) with overlaid segmentations (MRF: left image, Proposed: right image). Segmentation errors due to PV effects (red arrows) and disconnected cGM (yellow arrow). WM: red, cGM: dark blue, dGM: green, BS: light blue.

3.3 Connected Component Analysis

In addition to the visual inspection we calculated connected components (CC) of the segmentations. Ideally a segmentation would have seven connected components, one for each of the classes WM, cGM, DGM, CSF, CB, BS and BG. In practice it is obvious that the number of connected components is larger. In this experiment we focus on wrongly classified WM voxels which often create isles on the outer cGM boundary. For this purpose we calculated the number of total connected WM components (#CC) and the number of undesired connected WM components (#uCC).

With uCC we denote WM components that are adjacent both to cGM and CSF. The assumption is that these kind of components should not be present in a good segmentation. Table 1 shows how #CC and #uCC can be reduced using the proposed method. Having an average #uCC of 5.0 using second order neighborhood information is a significant improvement over the standard MRF method, where we observed in average 93 undesired components. Fig. 4 presents an age dependent analysis of the number of voxels belonging to a WM connected component that is not the largest component. This figure shows that the number of connected components increases with age. Due to increasing convolution of the cortex, occurrences of PV effects are more likely and thus the segmentation more challenging with increasing age. With the proposed method we are able to keep the number of voxels in undesired CCs low, even for higher ages. We point out that the explicit modeling of PV was not beneficial in the conducted tests.

	MRF	MRF (PV)	Proposed	Proposed (PV)
#CC	119 (±94)	160 (±113)	**48 (±44)**	78 (±57)
#uCC	93 (±74)	112 (±86)	**5.0 (±6.0)**	6.8 (±8.3)

Table 1. Connected component analysis: Average number of connected WM components, standard deviation in brackets.

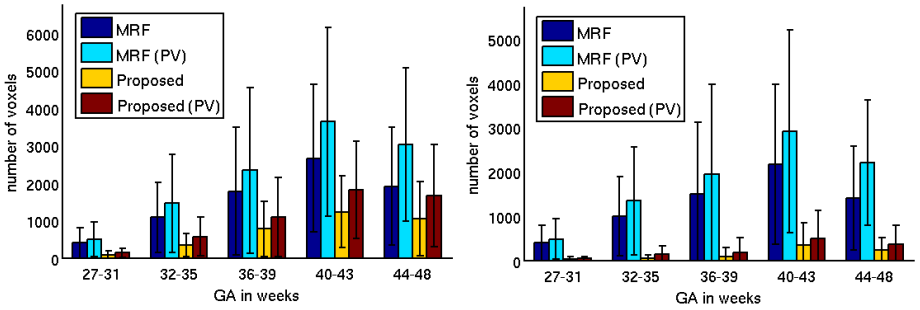

Fig. 4. Average number of voxels (bars) with standard deviation (error bars) that are not in the largest WM CC. Analysis for CC (left) and undesired CC (right).

4 Discussion and Future Work

As shown in [4, 5] an EM approach with the standard MRF is not sufficient to correct wrongly labeled PV voxels. We observed that if CSF and WM are modeled as non-adjacent classes, high MRF weight, the standard MRF approach with PV extension is able to potentially cope with the PV problem as well. There is also a need to model external CSF and internal CSF individually since internal CSF should be modeled as adjacent to WM. This distinction is not present in the available atlases [2, 4, 7, 12] and can be hard to define in general. In the future we are keen to compare the presented approach to the standard MRF modeling internal and external CSF individually.

Our experiments furthermore revealed no improvement by using explicit PV modeling. This is not surprising since the introduced PV class is initialized using the probabilities of the parent classes. For example, the PV class between cGM and CSF is initialized by the potentially low cGM and CSF probabilities and will thus not be able to compete against the WM class. This particular PV model seems not very well suited for this PV challenge arising in neonatal segmentation.

Regarding the choice of the parameters $\mathbf{T}_{\text{kjl}}$, we observed that with a reduced penalisation (smaller values) the desired PV correction effect is also reduced. On the other hand, in areas where due to unsharp priors low likelihoods of both neighboring classes j and l are falsely present, rather high values (≈ 5) for $\mathbf{T}_{\text{kjl}}$ seem to result in an unreasonably high penalisation and thus prevent a voxel of being correctly labeled as k.

The presented preliminary results look promising and we are planning to obtain manual segmentations to provide a thorough quantitative analysis.

5 Conclusion

We have presented a novel energy function that incorporates second order neighborhood information into the EM framework. We introduced a tensor $\mathbf{T}$ that penalizes labels with unexpected neighborhood configuration. In contrast to the standard MRF energy function, which is based on adjacency constraints between two different classes, we allow the specification of neighborhoods dependent on three different labels. We also adapted our model to the concept of modeling PV effects explicitly. Since no manually annotated ground truth segmentations were available, we evaluated our method both visually and numerically. While visual inspection clearly reveals the problem that our method tackles and the improvements obtained, numerical experiments confirm a significant improvement over the standard EM approach using first order MRFs.

References

1. M. Rutherford, "MRI of the neonatal brain," *Saunders Ltd.*, 2001.
2. A. Serag, P. Aljabar, G. Ball, et al., "Construction of a consistent high-definition spatio-temporal atlas of the developing brain using adaptive kernel regression," *NeuroImage*, vol. 59, no. 3, pp. 2255–2265, 2012.
3. F. Shi, Y. Fan, S. Tang, et al., "Neonatal brain image segmentation in longitudinal MRI studies," *NeuroImage*, vol. 49, no. 1, pp. 391–400, 2010.
4. M. Kuklisova-Murgasova, P. Aljabar, L. Srinivasan, et al., "A dynamic 4D probabilistic atlas of the developing brain," *NeuroImage*, vol. 54, no. 4, pp. 2750–2763, 2011.
5. H. Xue, L. Srinivasan, S. Jiang, et al., "Automatic segmentation and reconstruction of the cortex from neonatal MRI," *NeuroImage*, vol. 38, no. 3, pp. 461–477, 2007.
6. M. Prastawa, J. H. Gilmore, Weili Lin, and G. Gerig, "Automatic segmentation of MR images of the developing newborn brain," *Medical Image Analysis*, vol. 9, no. 5, pp. 457–466, 2005.
7. P. A. Habas, Kio Kim, J. M. Corbett-Detig, et al., "A spatiotemporal atlas of mr intensity, tissue probability and shape of the fetal brain with application to segmentation," *NeuroImage*, vol. 53, no. 2, pp. 460–470, 2010.
8. K. Van Leemput, F. Maes, D. Vandermeulen, and P. Suetens, "Automated model-based tissue classification of MR images of the brain," *IEEE TMI*, vol. 18, no. 10, pp. 897–908, 1999.
9. M. J. Cardoso, M. J. Clarkson, G. R. Ridgway, et al., "Load: A locally adaptive cortical segmentation algorithm," *NeuroImage*, vol. 56, no. 3, pp. 1386–1397, 2011.
10. S. M. Smith, "Fast robust automated brain extraction," *Human Brain Mapping*, vol. 17, no. 3, pp. 143–155, 2002.
11. N.J. Tustison, B.B. Avants, P.A. Cook, et al., "N4ITK: Improved N3 bias correction," *IEEE TMI*, vol. 29, no. 6, pp. 1310–1320, 2010.
12. F. Shi, P.-T. Yap, Y. Fan, et al., "Construction of multi-region-multi-reference atlases for neonatal brain MRI segmentation," *NeuroImage*, vol. 51, no. 2, pp. 684–693, 2010.